Heat Transfer at the Nanoscale: Evaporation of Nanodroplets

Robert Hołyst[1,2,*] and Marek Litniewski[1,†]

[1]*Institute of Physical Chemistry PAS, Kasprzaka 44/52, 01-224 Warsaw, Poland*

[2]*Cardinal Stefan Wyszyński University, WMP-College of Science Dewajtis, Warsaw, Poland*

(Received 27 August 2007; revised manuscript received 12 October 2007; published 8 February 2008)

We demonstrate using molecular dynamics simulations of the Lennard-Jones fluid that the evaporation process of nanodroplets at the nanoscale is limited by the heat transfer. The temperature is continuous at the liquid-vapor interface if the liquid/vapor density ratio is small (of the order of 10) and discontinuous otherwise. The temperature in the vapor has a scaling form $T(r, t) = T[r/R(t)]$, where $R(t)$ is the radius of an evaporating droplet at time t and r is the distance from its center. Mechanical equilibrium establishes very quickly, and the pressure difference obeys the Laplace law during evaporation.

DOI: 10.1103/PhysRevLett.100.055701 PACS numbers: 64.70.F−, 05.70.Ln, 68.03.Fg

In 1999, Feng and Ward [1] conducted a series of very precise measurements of the temperature distribution near the evaporating surface of water and found that the temperature is discontinuous at the interface, with the vapor temperature T_{vap} higher than the liquid temperature T_{liq}. This result contradicted the commonly accepted theories of evaporation [2–4] based on the linearized Boltzmann equation in a vapor phase. The authors concluded their paper as follows: "at present there does not appear to be any explanation for this observation from classical mechanics. It remains to be seen if quantum mechanics will provide an explanation." In 2004, Bond and Struchtrup [5] argued, using elements of kinetic theory of gases combined with elements of irreversible thermodynamics, that temperature discontinuity is strongly related to the energy flux during evaporation, a quantity grossly neglected in the theories of evaporation. They concluded that [5] the temperature discontinuity found in experiments [1,6] cannot be obtained from the classical Hertz-Knudsen or Schrage models of evaporation. The theories of evaporation which were developed and refined over the last 100 years [5,7], following the Maxwell paper [8], were based on approximations which focused on the mass transfer in vapor and underestimated the role of energy flux and energy balance during the evaporation process. Even today, the primary quantity of interest in the theoretical approach is the evaporation coefficient, condensation coefficient, accommodation coefficient, and the reflected flux of the vapor molecules [5,9–12]. Lack of careful experiments, such as those performed by Ward *et al.* [1,6,13,14], precluded proper verification of the theories against experimental results.

Here, we demonstrate in computer simulations of the Lennard-Jones (LJ) fluid that evaporation at the *nanoscale* is limited by heat transfer and energy balance at the liquid-gas interface and not by the mass diffusion inside the vapor (as assumed in the current theories). Our results agree quantitatively with the solution of irreversible thermodynamics in the two-phase region [15] for small liquid/vapor density ratio (of the order of 10). When this ratio is large, we observe large temperature discontinuity (as large as nearly 30% of liquid temperature) at the interface. In previous simulations [9,16–23] of evaporation performed for very small number of atoms (from 10^3 up to 10^5), the analysis of the heat transfer and energy balance analysis was not done. The results of our molecular dynamics simulations together with the solution of irreversible thermodynamics in the two-phase region [15] show a clear need for the reformulation of the current view on the dynamics of the evaporation.

We performed the molecular dynamics (MD) computer simulations for more than 10^6 Lennard-Jones atoms with the interaction potential truncated and shifted up to make the potential zero at $r = 2.5\sigma$, where σ, the Lennard-Jones diameter taken as 0.35 nm, set the length scale (for phase diagrams, see the supplementary information [24]). The Newton equations of motion were solved using the Verlet "leapfrog" scheme [25,26] with the time step $\delta t = 0.01\sigma(m/\varepsilon)^{1/2}$, where the energy unit was given by $\varepsilon = 112k_B$ K and mass of atoms at $m = 40$ amu. $\varepsilon/k_B = 112$ K set the temperature scale. The time unit was $t_u = \sigma(m/\varepsilon)^{1/2} \sim 2.3$ ps. Simulations of the evaporation process were performed for 5 equilibrium initial temperatures T_{eq} (changed from 0.68 to 0.9) leading to the liquid-vapor density ratio $\rho^0_{\mathrm{liq}}/\rho^0_{\mathrm{vap}}$ from 120 to 14. Three values of the boundary temperature T_b were considered (1.25, 1.75, and 2.5). The critical temperature in the system was roughly 1.1. Each simulation run started ($t = 0$) with a liquid droplet of radius $R(t = 0)$ (of sizes from 26.8 to 37.1) equilibrated with the surrounding gas and located in the center of the sphere of radius R_b (varied from 151 to 402). The gas particles were reflected elastically from the boundary of the sphere. Heating was done by scaling the particle velocity just after the reflection. The scaling factor was $(T_b/T_n)^{1/2}$ where T_n was the current value of the temperature of the gas enclosed between R_b and $R_b - 3$. During the evaporation process, the center of a droplet was fixed at the center of the sphere. Simulation runs were performed for the number of particles N from 746 414 to 2 691 050. In the simulations, the maximum value of the ratio $N_{\mathrm{liq}}/N_{\mathrm{vap}}$

(ratio of a number of atoms in the droplet to the one in vapor) at $t = 0$ was 0.143, typical value was 0.07–0.09, and the lowest one amounted to 0.023. For a few sets of initial parameters, simulation runs were repeated for different N, R_b, with no significant changes in the results. The energy per particle and the pressure in a liquid droplet, necessary to evaluate the enthalpy of evaporation, were measured (in a central part of the droplet) during simulation using standard formulas [25]. In order to evaluate the heat transfer, we determined the heat conductivity, κ_{vap}, in the vapor using a direct method proposed by Muller-Plathe [27], and as a check we used independent method proposed by Evans [25,28]. We found that κ_{vap} varied between 0.3 to 0.55 for different temperatures and densities (supplementary information [24]). The surface tension was determined in the independent simulations (for flat interface) from the difference between the normal and tangential pressure components [29] (supplementary information [24]).

The evolution of thermodynamic parameters during evaporation of a droplet can be conveniently divided into two regimes: a transient nonstationary regime and a quasistationary regime. Similar behavior was observed in the solution of irreversible thermodynamics equations in the two-phase region [15,30]. The first regime is associated with the process of heating the system. We observe that an initial sudden increase of T_{eq} to T_b at the boundary initiates a sound wave which moves from the wall to the surface of the droplet. The wave heats up a droplet from T_{eq} to $T_{\text{liq}}(T_{\text{liq}} \neq T_b)$. The heating process is due to the condensation of hot vapor at a colder surface of the droplet; thus, paradoxically, evaporation starts with initial condensation of vapor. Because of this condensation process, initially the droplet increases its temperature and size.

For our system, this initial transient period lasted for a time, t_0, of the order of few nanoseconds, but the time scale depended on the details of the heating process. Importantly, the stationary values of T_{liq} and ρ_{liq} were independent of the heating rate. An extra simulation run with scaling of velocities at the boundaries by the factor $(T_b/T_n)^{1/2}$ less than 1.004 (slow heating) led to exactly the same values of T_{liq} and ρ_{liq} as that for a factor 1.15 (fast heating). However, the first process characterized by slow heating lasted 10 times longer than the second one, and the droplet evaporated nearly 40% of its mass before reaching the quasistationary regime.

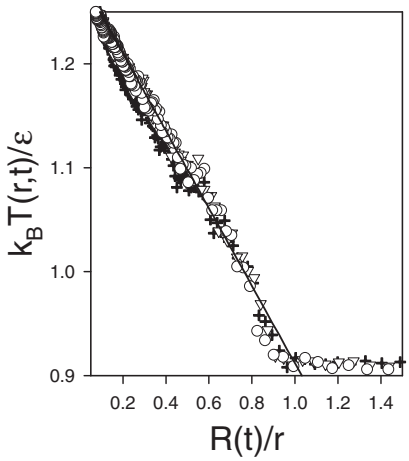

FIG. 1. Temperature, $T(r, t)$, versus inverse distance $[R(t)/r]$, normalized by the droplet radius $R(t)$ for liquid to vapor density ratio equal to 11 (r is a distance from the center of a droplet). The data are given for the evolution no. 5 from Table I at $t = 3000$, $R(t) = 24.6$ (empty circles); $t = 4000$, $R(t) = 22.3$ (empty triangles); $t = 5100$, $R(t) = 19.4$ (crosses). The solid line is given by Eq. (3) with $T_{\text{vap}} = T_{\text{liq}}$.

In the quasistationary regime, T_{liq} and ρ_{liq} were constant, and the temperature profile in the vapor obeyed scaling relation $T(r, t) = T[r/R(t)]$ for $R_b \gg R(t)$. We observed that the temperature distribution and evaporation rate strongly depended on the magnitude of liquid-vapor density ratio $\rho^0_{\text{liq}}/\rho^0_{\text{vap}}$. First, we consider a case when $\rho^0_{\text{liq}}/\rho^0_{\text{vap}}$ was smaller than roughly 20. In this case, the temperature was continuous at the interface $T[r = R(t)] = T_{\text{vap}} = T_{\text{liq}}$. We found that the temperature profile obtained in the simulations was well described by the following equation (from irreversible thermodynamics [15]):

$$\partial_r(r^2 \kappa_{\text{vap}} \partial_r T) = 0, \tag{1}$$

with the boundary conditions given by

$$T[r = R(t)] = T_{\text{vap}} \qquad T(r = R_b) = T_b. \tag{2}$$

The solution to Eq. (1) (for κ_{vap} constant) reads as follows:

$$T(r, t) = [R_b T_b - R(t) T_{\text{vap}} - R_b R(t)(T_b - T_{\text{vap}})/r]/[R_b - R(t)] \quad \text{for } r \geq R(t) \tag{3}$$

and $T(r, t) = T_{\text{liq}} = T_{\text{vap}}$ for $r < R(t)$. In Fig. 1, we show a comparison of the simulation results with Eq. (3).

In the second case, when $\rho^0_{\text{liq}}/\rho^0_{\text{vap}} > 30$, we found that temperature was discontinuous at the interface (shown in Fig. 2) with the vapor temperature T_{vap} larger than the liquid temperature T_{liq}. The difference $T_{\text{vap}} - T_{\text{liq}}$ grew as we decreased the vapor density and increased the liquid density (Table I). The temperature profile was quasistationary also in this case; i.e., $T(r, t) = T[r/R(t)]$ as shown in Fig. 2, but it deviated from the $1/r$ dependence given in Eq. (3). The observed deviations of the temperature profile from Eq. (3) (Figs. 1 and 2) could arise (i) from the dependence of the heat conductivity on temperature [see Eq. (1)] and (ii) from a constraint of mechanical equilibrium.

In all studied cases (presented in Table I), we analyzed the evaporation rate on the basis of the heat transfer and energy balance equation at the interface:

$$-\rho_{\text{liq}} \Delta H \partial_t R = \kappa_{\text{vap}} (\partial_r T)_{r=R(t)}. \tag{4}$$

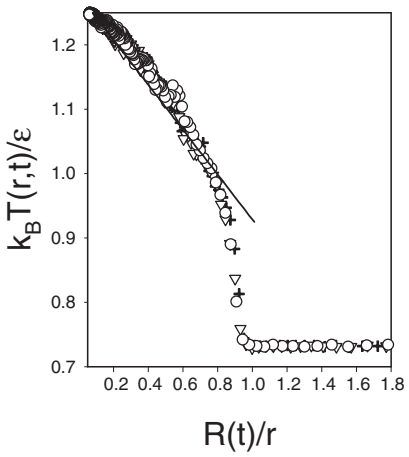

FIG. 2. Legend as in Fig. 1. Liquid-vapor density ratio is equal to 119. The data are taken from the evolution no. 1 from Table I. Here, $t = 10450$, $R(t) = 31.9$ (empty circles); $t = 16300$, $R(t) = 27.5$ (empty triangles); $t = 20470$, $R(t) = 24.1$ (crosses). The solid line is a theoretical line given by Eq. (3) with $T_{\rm vap} = T_{\rm liq} + 0.195$.

On the left-hand side, the mass flux $-\rho_{\rm liq}\partial_t R$ into the vapor is multiplied by the enthalpy change ΔH (per particle) upon evaporation. The energy flux into the vapor is compensated by the heat flux given on the left-hand side of Eq. (4) by the heat conductivity at the interface multiplied by the temperature gradient at the interface, $\kappa_{\rm vap}(\partial_r T)_{r=R(t)}$. Inserting Eq. (3) into (4) gives the following relation for $R(t)$:

TABLE I. Results for experimental and theoretical values W_E and W_T, respectively. W_T—theoretical value of the slope of $[R^*(t)]^2$ $(R^*(t)^2 = R(t)^2[1 - 2R(t)/(3R_b)])$ versus t given by Eq. (6). W_E—experimental value of the slope taken from fitting $[R^*(t)]^2$ with a straight line after the initial transient regime ($t > t_0$) (see Figs. 3 and 4). $T_{\rm vap}$—vapor temperature at the interface taken from the fit of $T(r)$ to Eq. (3) (see Figs. 1 and 2). $T_{\rm eq}$, $\rho^0_{\rm vap}$—initial (equilibrium) temperature and vapor density. T_b—temperature at the boundary; $T_{\rm liq}$, $\rho_{\rm liq}$—temperature and density measured in central parts of droplets during evaporation. Here, $\Delta h = h(\rho^0_{\rm vap}, T_{\rm vap}) - h(\rho_{\rm liq}, T_{\rm liq})$ is the change of enthalpy upon evaporation. We find that $W_E \approx W_T$, supporting our conclusion that heat transfer is a limiting factor for evaporation. Note that the slope changed 1 order of magnitude in the simulations (first and last row of the Table). In simulations, no. 1–5, we decrease liquid-vapor density ratio $(\rho_{\rm liq}/\rho^0_{\rm vap})$ up to a point where the temperature jump disappears (the wall temp. was set at 1.25) which occurs at the density ratio of the order of 10. For such small density ratio (simulations 5–9), we do not observe temperature jump even when the boundary temperature T_b is as high as 2.5.

	$T_{\rm eq}$	$\rho^0_{\rm vap}$	T_b	$T_{\rm liq}$	$\rho_{\rm liq}$	Δh	W_E	W_T	$T_{\rm vap} - T_{\rm liq}$
1	0.679	0.0065	1.25	0.731	0.776	5.865	0.043	0.055	0.195
2	0.713	0.0096	1.25	0.768	0.756	5.594	0.054	0.062	0.151
3	0.758	0.0148	1.25	0.816	0.727	5.234	0.068	0.072	0.097
4	0.800	0.0219	1.25	0.863	0.696	4.832	0.080	0.085	0.050
5	0.851	0.0327	1.25	0.912	0.662	4.391	0.100	0.104	0.0
6	0.851	0.0327	1.75	0.963	0.621	4.157	0.284	0.284	0.0
7	0.851	0.0327	2.50	1.017	0.564	3.842	0.627	0.659	0.0
8	0.903	0.0484	1.25	0.971	0.611	3.923	0.133	0.122	0.0
9	0.903	0.0484	1.75	1.031	0.544	3.569	0.454	0.407	0.0

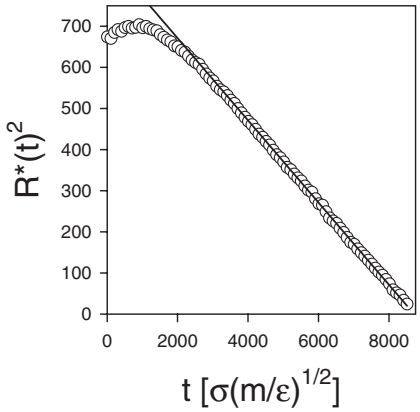

FIG. 3. $R^*(t)^2 = R(t)^2[1 - 2R(t)/(3R_b)]$ versus time, t, for the evolution no. 5 from Table I. The empty circles give simulation data. The solid line is the theoretical result given by Eq. (6).

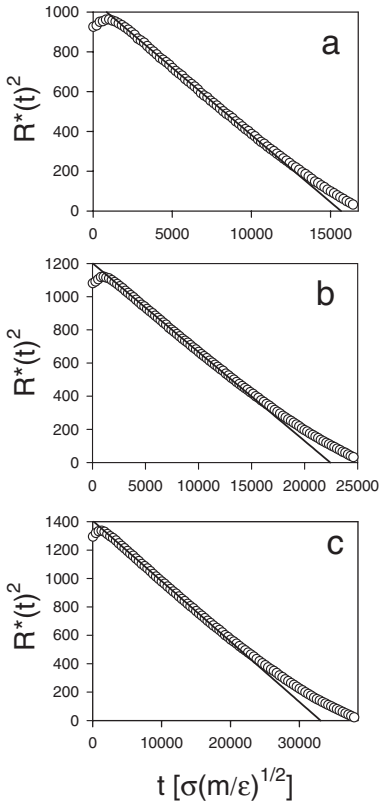

FIG. 4. $R^*(t)^2$ versus time, t for large liquid-vapor density ratio and different mean-free path of atoms in the vapor, $\lambda \approx (\pi\sigma^2\rho_{\rm vap})^{-1}$. The empty circles give the simulation data. The solid line is given by Eq. (6). (a) evolution no. 3 from Table I. $\lambda \approx 21.5$; (b) evolution no. 2 from Table I, $\lambda \approx 33.2$; (c) evolution no. 1 from Table I $\lambda \approx 49$. Deviations from Eq. (6) are observed when the diameter of the droplet becomes smaller than 1 mean free path $[2R(t) < \lambda]$.

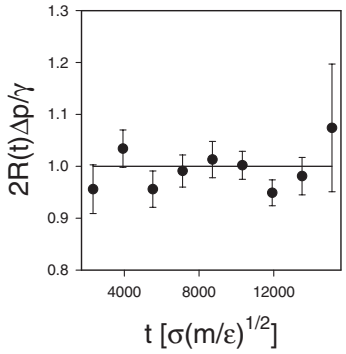

FIG. 5. The pressure difference inside or outside the droplet, $\Delta p = p_{\mathrm{liq}} - p_{\mathrm{vap}}$ normalized by the Laplace value $2\gamma/R(t)$, is shown as a function of time t for the evolution no. 3 in Table I.

$$R(t)^2[1 - 2R(t)/(3R_b)] = R(t_0)^2[1 - 2R(t_0)/(3R_b)] - 2\kappa_{\mathrm{vap}}(T_b - T_v)/(\rho_{\mathrm{liq}}\Delta H) \times (t - t_0). \quad (5)$$

For $R(t) \ll R_b$, we get a linear relation $R^2(t) - R^2(t_0) = -W_T(t - t_0)$, where

$$W_T = 2\kappa_{\mathrm{vap}}(T_b - T_{\mathrm{vap}})/(\rho_{\mathrm{liq}}\Delta H). \quad (6)$$

Here, κ_{vap} is the heat conductivity at temperature T_{vap}. Figures 3 and 4 and Table I show comparison between simulation and theory [Eqs. (5) and (6)]. All thermodynamic parameters in W_T were determined independently, and theoretical formula does not contain any free fitting parameters. Please note that Eq. (4) is very restrictive. In principle, evaporation could proceed with a decrease of droplet temperature without a need for an energy flux from the vapor.

Mechanical equilibrium established very quickly in comparison to thermal equilibrium. The Laplace's law was obeyed during the evaporation as shown on Fig. 5 (see also Fig. S3 in supplementary information [24]). Since the evaporation flux is governed by the chemical potential difference which is a function of temperature and pressure, we conclude that evaporation follows the change of temperature and not that of pressure. Additionally, the condition of mechanical equilibrium,

$$\Delta p = p_{\mathrm{liq}}(T_{\mathrm{liq}}, \rho_{\mathrm{liq}}) - p_{\mathrm{vap}}(T[r/R(t)], \rho_{\mathrm{vap}}[r/R(t)]) = 2\gamma/R(t), \quad (7)$$

gives the constraint on possible profiles of temperature and density.

We demonstrated that the evaporation process is limited by the heat transfer and energy balance condition.

This work was supported by the Ministry of Science and Higher Education as a scientific project No. 2007-2009. R. H. acknowledges support from the Foundation for Polish Science.

*holyst@ptys.ichf.edu.pl
†mark@ichf.edu.pl

[1] G. Fang and C. A. Ward, Phys. Rev. E **59**, 417 (1999); **59**, 441 (1999).
[2] Y.-P. Pao, Phys. Fluids **14**, 306 (1971); **14**, 1340 (1971); **16**, 1560 (1973).
[3] J. W. Cipolla, Jr., H. Lang, and S. K. Loyalka, J. Chem. Phys. **61**, 69 (1974).
[4] D. Bedaux, L. F. Hermans, and T. Ytrehus, Physica A (Amsterdam) **169**, 263 (1990).
[5] M. Bond and H. Struchtrup, Phys. Rev. E **70**, 061605 (2004).
[6] C. A. Ward and D. Stanga, Phys. Rev. E **64**, 051509 (2001).
[7] R. W. Schrage, *A Theoretical Study of Interphase Mass Transfer* (Columbia University Press, New York, 1953).
[8] J. C. Maxwell, Philos. Trans. R. Soc. Lond. **170**, 231 (1879).
[9] T. Ishiyama, T. Yano, and S. Fujikawa, Phys. Rev. Lett. **95**, 084504 (2005).
[10] R. Meland, A. Frezzotti, T. Ytrehus, and B. Hafskjold, Phys. Fluids **16**, 223 (2004).
[11] S. S. Sazin, Prog. Energy Combust. Sci. **32**, 162 (2006).
[12] K. K. Kuo, *The Principles of Combustion* (John Wiley & Sons, New York, 1986).
[13] C. A. Ward and F. Duan, Phys. Rev. E **69**, 056308 (2004).
[14] F. Duan and C. A. Ward, Phys. Rev. E **72**, 056302 (2005).
[15] V. Babin and R. Hołyst, J. Phys. Chem. B **109**, 11367 (2005).
[16] K. Yasuoka and M. Matsumoto, J. Chem. Phys. **101**, 7904 (1994).
[17] L. N. Long, M. M. Micci, and B. C. Wong, Comput. Phys. Commun. **96**, 167 (1996).
[18] J. H. Walther and P. Koumoutsakos, J. Heat Transfer **123**, 741 (2001).
[19] P. Yi, D. Poulikakos, J. Walther, and G. Yadigaroglu, Int. J. Heat Mass Transf. **45**, 2087 (2002).
[20] G. K. Schenter, S. M. Kathmann, and B. C. Garrett, Phys. Rev. Lett. **82**, 3484 (1999).
[21] S. I. Anisimov, D. O. Dunikov, V. V. Zhakhovskii, and S. P. Malyshenko, J. Chem. Phys. **110**, 8722 (1999).
[22] T. Tsuruta, H. Tanak, and T. Masuoka, Int. J. Heat Mass Transf. **42**, 4107 (1999).
[23] L. Consolini, S. K. Aggarwal, and S. Murad, Int. J. Heat Mass Transf. **46**, 3179 (2003).
[24] See EPAPS Document No. E-PRLTAO-100-010806 for supplementary information. For more information on EPAPS, see http://www.aip.org/pubservs/epaps.html.
[25] M. P. Allen and D. J. Tildesley, *Computer Simulations of Liquids* (Oxford University, Oxford, 1987).
[26] L. Verlet, Phys. Rev. **159**, 98 (1967).
[27] F. Muller-Plathe, J. Chem. Phys. **106**, 6082 (1997).
[28] D. J. Evans, Phys. Lett. A **91**, 457 (1982).
[29] B. Shi, S. Sinha, and V. K. Dhir, J. Chem. Phys. **124**, 204715 (2006).
[30] V. Babin and R. Hołyst, J. Chem. Phys. **122**, 024713 (2005).